University of Reading
School of Mathematics, Meteorology & Physics

Examination of non-Time Harmonic Radio Waves Incident on Plasmas

by

Andrew Ash

August 2008

This dissertation is submitted to the Department of Mathematics in partial fulfilment of the requirements for the degree of Master of Science

Abstract

The examination of radio waves propagating, interacting and reflecting off various bodies and materials is of interest in many areas of research, including assessing radio communications through the ionosphere, determining effects on soft tissue from mobile phone use and producing radar cross section estimates for military purposes. Analytical solutions exist for only the simplest of geometries where Maxwell's equation can be solved, so to fulfil all of these diverse requirements numerical techniques have been developed, and one such method is the Finite Difference Time Domain through thpul use any at,)Tj-0.0004 Tc 0.0026 Tj 690025

DECLARATION

I confirm that this is my own work and the use of all material from other sources has been properly and fully acknowledged.

Signed………………………………………….. (Andrew Ash)

Acknowledgements

I wish to thank Steve Langdon for his assistance and direction while completing this dissertation. I also wish to thank my employer, Defence Science and Technology Laboratory (Dstl) for the financial and managerial support while completing my Masters.

Contents

1. Introduction

The generation of radio waves for the purpose of detecting objects at a distance from an observation point, known as Radio Detection and Ranging (RADAR), has been utilised since the early 20th century for both civilian and military purposes. In basic geometrical shapes is presented in the Radar Cross Section Handbook by Ruck [4]. This also includes methods for obtaining the RCS of complex objects made from superimposing a number of simple shapes together. Additionally analytical solutions for the RCS of non-perfectly conducting materials are discussed, with reference to plasmas and the analytical solution of plasma spheres given by Mie [10]. The book by K. S. Kunz and R. J. Luebbers [1] provides a detailed background in the formulation of numerical methods used to predict RCS and radar signatures of various objects, in particular utilising Finite

Research into plasma and its interaction with electromagnetic waves has been ongoing for almost as long as the use of FDTD. The added difficulty when trying to consider real rather than theoretical perfect plasmas is the need to determine the accurate Total Electron Content (TEC) within a region and how it evolves with time. Reference [2] gives some detailed background theory on plasma behaviour. Due to the need of additional numerical (usually Monte-Carlo, Computational Fluid Dynamics (CFD)) computer codes to determine the plasma behaviour, a computer code to determine the RCS of a plasma object is usually de-coupled from the code that will generate the TEC evolution within the region of interest.

From the literature examined in the course of this work, it is apparent that the determination of RCS values for a number of objects is well practised and documented. This has utilised FDTD (in various forms) to examine RCS values at a range of frequencies using time harmonic incident radio waves modelled in the computational domain. The aim of this project is to examine the use of non-time harmonic waves (utilised by a large number of modern, pulse compression radar systems in the form of a ‘chirp’ pair) to interrogate objects shielded by plasma. In particular, the effect of space steps on the error of the solution in modelling a chirped pulse is examined.

The remainder of this report is structured as follows: -

Section 2 discusses some general electromagnetic theory, in particular the Maxwell equations which govern the propagation of radio waves through a medium.

Section 3 investigates analytical solutions of electromagnetic waves travelling in free space, incident on a Perfectly Electrical Conducting (PEC) surface and obliquely incident on a dielectric medium.

2. Electromagnetic Theory

The propagation of electromagnetic waves is governed by four Maxwell equations. These describe the relations between the electric (E) and magnetic (H) fields and are applicable to electromagnetic wave propagation in both free space and in various media.

Consider a three dimensional problem in which [illegible] (ween the elecpaceic (

(1)

$x \quad y \quad z$

$x \quad y \quad z$

Equations (3) and (4) are contained within (5) and (6), which can be shown by considering the divergence of each. Firstly, we take the divergence of equation (5): -

$$\nabla \cdot \nabla \times \underline{E} = \nabla \cdot \frac{-\partial \underline{B}}{\partial t} \;. \tag{7}$$

The divergence of a curl of a vector field is zero; this is shown in Appendix A, Lemma 1, so we use the identity: -

$$\nabla \cdot \nabla \times \underline{E} = 0 \,, \tag{8}$$

Therefore, returning to (7) we see that we have: -

$$0 = -\frac{\partial}{\partial t} \nabla \cdot \underline{B} \quad . \tag{9}$$

This implies that the divergence of the magnetic field B is constant with time. Without loss of generality we set B to be zero at t = 0, and hence this implies that the divergence of B is zero at all times.

Similarly, taking the divergence of (6) and again using Appendix A, Lemma 1: -

$$\nabla \cdot \left(\nabla \times \underline{B}\right) = \mu \nabla \cdot \underline{J} + \mu\varepsilon \nabla \cdot \frac{\partial \underline{E}}{\partial t} \quad , \tag{10}$$

$$\Rightarrow 0 = \nabla \cdot \underline{J} + \varepsilon \frac{\partial}{\partial t} \nabla \cdot \underline{E} \quad , \tag{11}$$

$$\Rightarrow \varepsilon \frac{\partial}{\partial t} \left(\nabla \cdot \underline{E}\right) = -\nabla \cdot \underline{J} \quad . \tag{12}$$

$$\nabla \cdot \underline{J} = -\frac{\partial \rho}{\partial t} \, , \tag{13}$$

which when substituted into (12) gives: -

$$, \tag{14}$$

3. Analytical Solutions

and t is the time in seconds. From standard wave theory, c=fλ, where f is the frequency and λ is the wavelength of the electromagnetic wave.

The associated magnetic field is given by: -

$$\underline{H} = \underline{H}_0 \cos(\kappa + \omega t - kz), \quad \textbf{(26)}$$

i.e. the magnetic fields are in phase with the electric fields, and have the same wavenumber (and therefore the same wavelength and frequency). Figure 2 shows the arrangement of electric and magnetic fields in the plane wave.

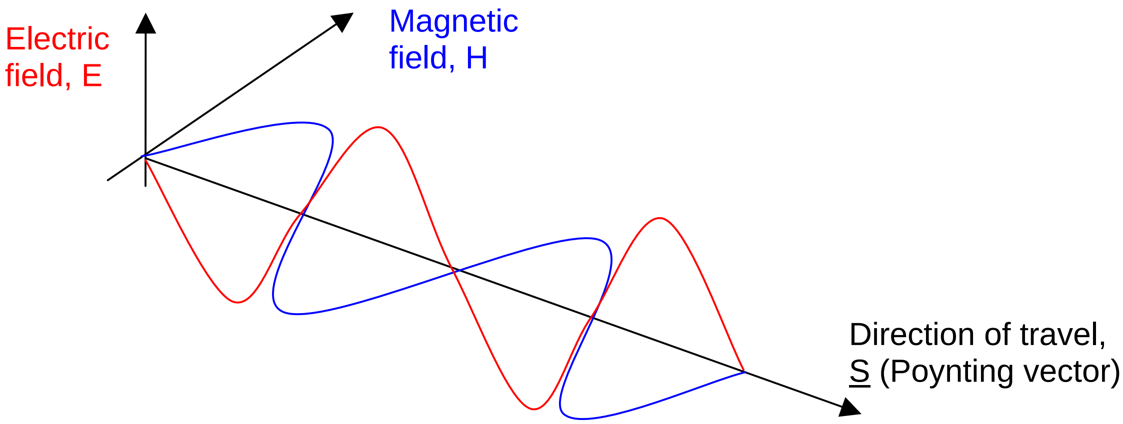

3.2. Plane Wave Incident on a PEC Plane

When examining the scattering of an electromagnetic wave off a solid object, it is often assumed that the target being interrogated is made of Perfectly Electrical Conductor (PEC). Essentially this means that the target comprises of a material that is close to a perfect conductor, such that electromagnetic waves incident on the target are reflected away with no appreciable degradation in amplitude of the incident wave. Explicitly, PEC can be characterized as follows: -

Electrical Permittivity, $\varepsilon_r \to \infty$.

Many metals commonly used in the construction of airframes, such as aluminium and titanium, have extremely high electrical permittivities for a large range of frequencies incident upon them, and as such may be approximated by PEC.

3.3 Plane Wave Obliquely Incident on a Dielectric Surface

We consider an electromagnetic plane wave incident on a dielectric material at an angle ς_i to the normal of the surface. The effect of having a dielectric material rather than a PEC surface is that the its electrical permittivity is of a similar order of magnitude compared to the permittivity of free space, ε_0, with a relative permittivity, ε_r, greater than one. Figure 3 shows this arrangement, where we have the electric field, E_x, perpendicular to the surface that it is incident upon. The superscript i denotes the incident wave electric and magnetic fields, t denotes the transmitted wave and r denotes the reflected wave: -

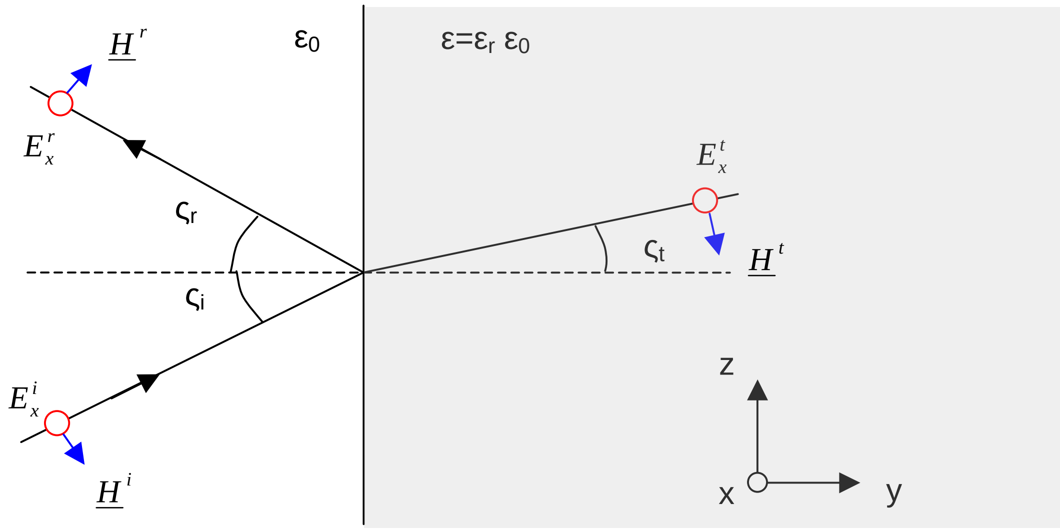

Figure 3: Plane wave obliquely incident on a dielectric

Standard theory from electromagnetics [3] is used to solve this situation to give expressions for the magnitude of the transmitted and reflected electric field component of the electromagnetic wave and the direction of travel relative to the normal of the material (ς_t). These are known as the perpendicular Fresnel equations ((28) and (29)) and Snell's laws ((30) and (31)) respectively [3]: -

$$\left|\quad\right| \quad \left|\quad\right| \frac{\left(\sqrt{\quad}\cos\quad\right)^{-1} \quad \left(\cos\quad\right)^{-1}}{\left(\sqrt{\quad}\cos\quad\right)^{-1} \quad \left(\cos\quad\right)^{-1}} \quad , \qquad \textbf{(28)}$$

$$\left|\quad\right| = \left|\quad\right| \frac{2\left(\sqrt{\quad}\cos\quad\right)^{-1}}{\left(\sqrt{\quad}\cos\quad\right)^{-1} + \left(\cos\quad\right)^{-1}} \quad , \qquad \textbf{(29)}$$

We can also use this method to produce equations for the magnetic field in the x, y and z components.

$$\mu\frac{-\partial \underline{H}}{\partial t} = \begin{vmatrix} \underline{i} & \underline{j} & \underline{k} \\ \frac{\partial}{\partial x} & \frac{\partial}{\partial y} & \frac{\partial}{\partial z} \\ E_x & E_y & E_z \end{vmatrix} - \sigma^* \underline{H} \quad , \tag{40}$$

Here, we have modified equation (3) to include a magnetic loss term (σ*H terms, where σ* is the magnetic conductivity), which is analogous to the electric loss term represented by σE in equation (36). These terms allow the possibility of the region in which the electromagnetic waves propagate to induce a magnetic loss. Equating terms in the i, j and k directions we obtain equations (41) to (43): -

$$\mu\frac{-\partial H_x}{\partial t} = \frac{\partial E_z}{\partial y} - \frac{\partial E_y}{\partial z} - \sigma^* H_x \quad , \tag{41}$$

$$\mu\frac{-\partial H_y}{\partial t} = \frac{\partial E_x}{\partial z} - \frac{\partial E_z}{\partial x} - \sigma^* H_y \quad , \tag{42}$$

$$\mu\frac{-\partial H_z}{\partial t} = \frac{\partial E_y}{\partial x} - \frac{\partial E_x}{\partial y} - \sigma^* H_z \quad . \tag{43}$$

In this project we will only be considered lo size $\Delta x \Delta y \Delta z$, where Δx, Δy and Δ

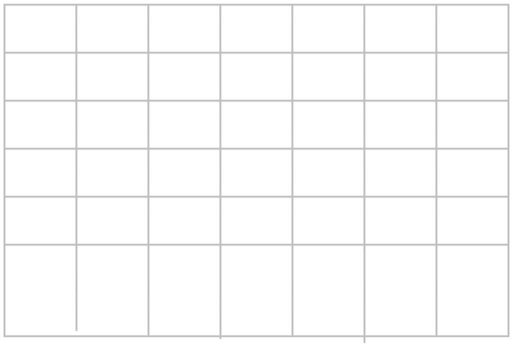

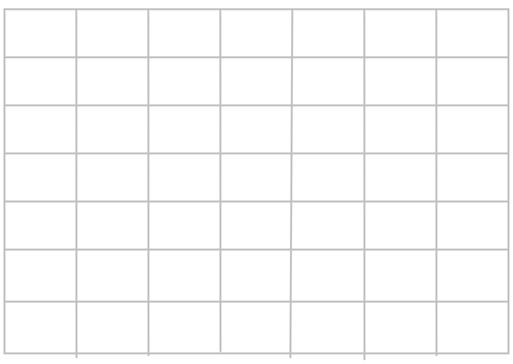

differences to approximate the six equations (37) to (39) and (41) to (43) which describe electromagnetic propagation in 3 dimensions: -

$$\mu \frac{H_x\big|^{n+}_{m\,p\,q} - H_x\big|^{n}_{m\,p\,q}}{\Delta t} = \frac{E_y\big|^{n+-}_{m\,p\,q+} - E_y\big|^{n+-}_{m\,p\,q}}{\Delta z} - \frac{E_z\big|^{n+-}_{m\,p+\,q} - E_z\big|^{n+-}_{m\,p\,q}}{\Delta y}$$

$$\mu \frac{H_y\big|^{n+}_{m\,p\,q} - H_y\big|^{n}_{m\,p\,q}}{\Delta t} = \frac{E_z\big|^{n+-}_{m+\,p\,q} - E_z\big|^{n+-}_{m\,p\,q}}{\Delta x} - \frac{E_x\big|^{n+-}_{m\,p\,q+} - E_x\big|^{n+-}_{m\,p\,q}}{\Delta z}$$

$$\mu \frac{H_z\big|^{n+}_{m\,p\,q} - H_z\big|^{n}_{m\,p\,q}}{\Delta t} = \frac{E_x\big|^{n+-}_{m\,p+\,q} - E_x\big|^{n+-}_{m\,p\,q}}{\Delta y} - \frac{E_y\big|^{n+-}_{m+\,p\,q} - E_y\big|^{n+-}_{m\,p\,q}}{\Delta x}$$

$$\varepsilon \frac{E_x\big|^{n+}_{m\,p\,q} - E_x\big|^{n}_{m\,p\,q}}{\Delta t} = \frac{H_z\big|^{n+-}_{m\,p+\,q} - H_z\big|^{n+-}_{m\,p\,q}}{\Delta y} - \frac{H_y\big|^{n+-}_{m\,p\,q+} - H_y\big|^{n+-}_{m\,p\,q}}{\Delta z} - \sigma E_x$$

$$\varepsilon \frac{E_y\big|^{n+}_{m\,p\,q} - E_y\big|^{n}_{m\,p\,q}}{\Delta t} = \frac{H_x\big|^{n+-}_{m\,p\,q+} - H_x\big|^{n+-}_{m\,p\,q}}{\Delta z} - \frac{H_z\big|^{n+-}_{m+\,p\,q} - H_z\big|^{n+-}_{m\,p\,q}}{\Delta x} - \sigma E_y$$

$$\varepsilon \frac{E_z\big|^{n+}_{m\,p\,q} - E_z\big|^{n}_{m\,p\,q}}{\Delta t} = \frac{H_y\big|^{n+-}_{m+\,p\,q} - H_y\big|^{n+-}_{m\,p\,q}}{\Delta x} - \frac{H_x\big|^{n+-}_{m\,p+\,q} - H_x\big|^{n+\frac{1}{2}}_{m\,p\,q}}{\Delta y} - \sigma E_z$$

fields within the bulk of the computational domain are calculated, using explicit expressions for the n=1 E-fields (52) to (54) based on the n=1/2 H-fields. After all these have been determined, the magnetic fields within the bulk of the domain are determined for the n=3/2 time step using the newly calculated n=1 E-fields (equations (55) to (57)). This process is repeated at each time step to get from the n to n+1, producing a leap-frog method in which E-fields are determined using the n+1/2 H-fields, and the H-fields from the n E-fields; as described by equations (52) to (57).

$$+\frac{\Delta}{\quad}$$ ®

$$H_x\Big|_{m,p,q}^{n+\frac{3}{2}} = H_x\Big|_{m,p,q}^{n+\frac{1}{2}} + \frac{\Delta t}{\mu}\frac{E_y\Big|_{m,p,q+1}^{n+1} - E_y\Big|_{m,p,q}^{n+1}}{\Delta z} - \frac{\Delta t}{\mu}\frac{E_z\Big|_{m,p+1,q}^{n+1} - E_z\Big|_{m,p,q}^{n+1}}{\Delta y} \quad \textbf{(55)}$$

$$H_y\Big|_{m,p,q}^{n+\frac{3}{2}} = H_y\Big|_{m,p,q}^{n+\frac{1}{2}} + \frac{\Delta t}{\mu}\frac{E_z\Big|_{m+1,p,q}^{n+1} - E_z\Big|_{m,p,q}^{n+1}}{\Delta x} - \frac{\Delta t}{\mu}\frac{E_x\Big|_{m,p,q+1}^{n+1} - E_x\Big|_{m,p,q}^{n+1}}{\Delta z} \quad \textbf{(56)}$$

$$H_z\Big|_{m,p,q}^{n+\frac{3}{2}} = H_z\Big|_{m,p,q}^{n+\frac{1}{2}} + \frac{\Delta t}{\mu}\frac{E_x\Big|_{m,p+1,q}^{n+1} - E_x\Big|_{m,p,q}^{n+1}}{\Delta y} - \frac{\Delta t}{\mu}\frac{E_y\Big|_{m+1,p,q}^{n+1} - E_y\Big|_{m,p,q}^{n+1}}{\Delta x} \quad \textbf{(57)}$$

4.3. Boundary Conditions

The FDTD equations (52) to (57) are such that each of the explicit electric/magnetic field equations require values for the magnetic/electric field around (spatially) the point being considered. As such, the arrangement of the Yee cells within the computational grid will result in a ‘missing’ electric/magnetic field at the edge of the computational domain, as demonstrated in Figure 7, representing the y = 0 plane: -

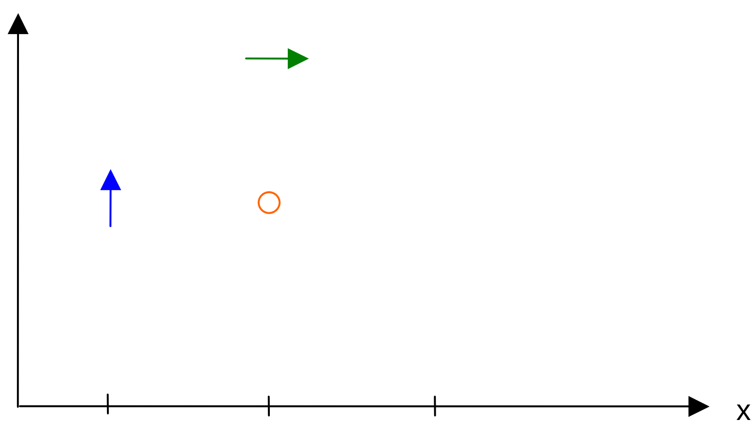

<u>x=MΔx</u>

$$E_y\Big|^{n\;\;1}_{M,p,q} = E_y\Big|^{n}_{M\;\;1,p,q} + \frac{c\Delta t - \Delta x}{c\Delta t + \Delta x}\left(E_y\Big|^{n+1}_{M\;\;1,p,q} - E_y\Big|^{n}_{M,p,q}\right) \quad , \tag{64}$$

$$E_z\Big|^{n+1}_{M,p,q} = E_z\Big|^{n}_{M-1,p,q} + \frac{c\Delta t - \Delta x}{c\Delta t + \Delta x}\left(E_z\Big|^{n+1}_{M-1,p,q} - E_z\Big|^{n}_{M,p,q}\right) \quad , \tag{65}$$

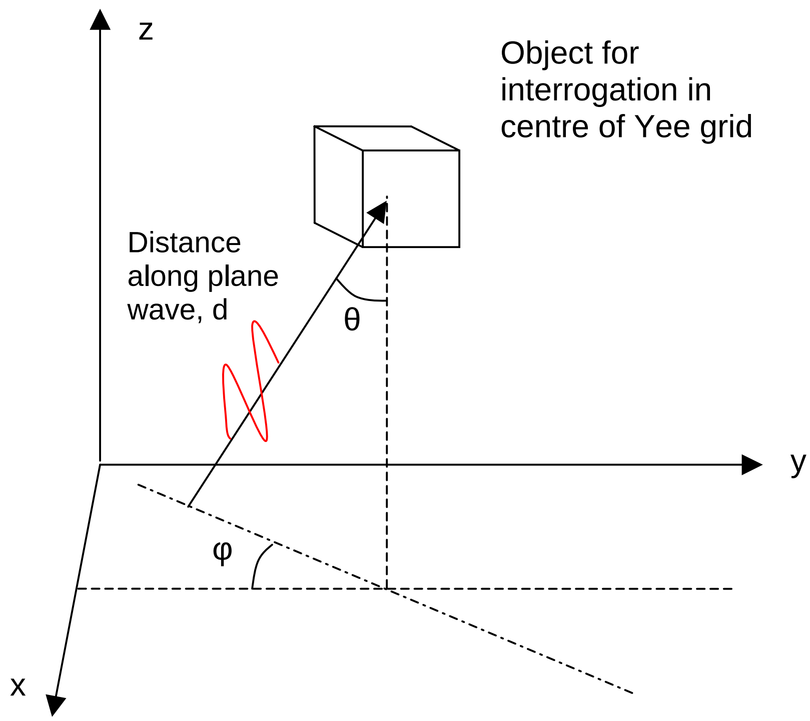

Figure 8: Arrangement of incident wave relative to computational grid

The incident wave will be varied such that it approaches the object from various angles relative to the z-direction in the grid, denoted by θ. This will allow the back-scattered radiation from different aspect angles to be determined, i.e. to give an electric field profile against aspect (viewing) angle. The incident wave will also be rotated about the z-axis, denoted by φ, such that the effect of the Yee grid, i.e. of using a series of cubes to represent a smooth object, can be negated by averaging over these viewing angles. We introduce three Euler angles: -

ψ – a rotation of the incident beam electric and magnetic fields in the x-y plane,
θ – a rotation of the incident beam direction in the y-z plane,
φ – a rotation of the incident beam direction in the x-y plane.

As finite differences are being used in this simulation, discontinuities in electric and/or magnetic fields will tend to produce spurious results and as such a wave that is ‘square’ (finite in size with zero values on its boundary) will propagate in several directions and be incoherent after a few time steps.

In this problem the incident wave is chosen to be a cylindrical wave, which is Gaussian in a radial direction and spatially along the initial wave. A schematic of this is shown in Figure 9: -

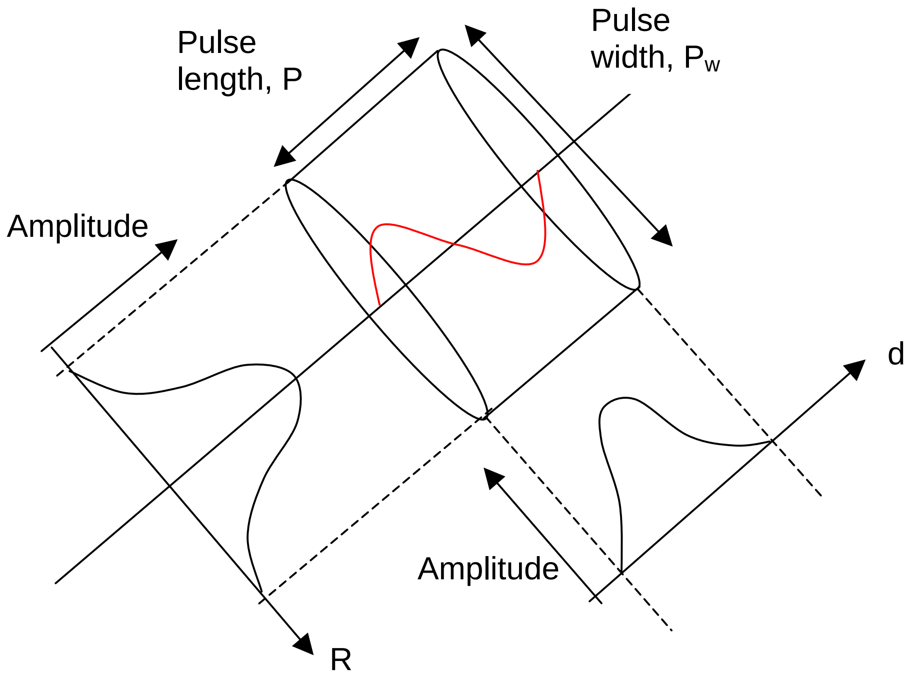

Figure 9: Schematic of incident radar pulse, showing radial and spatial amplitudes

This arrangement for the incident wave is intended to reduce the spurious behaviour at the edge of the wave packet. The amplitude factors, α (along direction of travel) and β (radial from centre of

where, $\nu = \sqrt{\dfrac{\mu_0}{\varepsilon_0}}$, **(77)**

gives the free space impedance. Combining this information with the transformation defined in (75) we can derive the six initial wave amplitudes in the x, y and z component directions: -

$$E_x = E_0(\sin\psi\cos\varphi + \cos\psi\cos\theta\sin\varphi) \qquad H_x = -\frac{E_0}{\nu}(\cos\psi\cos\varphi - \sin\psi\cos\theta\sin\varphi)$$
$$E_y = E_0(-\sin\psi\sin\varphi + \cos\psi\cos\theta\cos\varphi) \qquad H_y = -\frac{E_0}{\nu}(-\cos\psi\sin\varphi - \sin\psi\cos\theta\cos\varphi)$$
$$E_z = E_0(-\cos\psi\sin\theta) \qquad H_z = -\frac{E_0}{\nu}(\sin\psi\sin\theta) \quad . \ \mathbf{(78)}$$

The approximation we will use in the formulation of the incident electric field wave can be explicitly described as: -

$$E_x\big|_{m,p,q}^{0} \approx E_x(\underline{r}), \quad \mathbf{(79)}$$

where $\underline{r} = \underline{i}(m\Delta x) + \underline{j}(p\Delta y) + \underline{k}(q\Delta z)$. **(80)**

The spatial components of the wave in the initial conditions of the problem are given by (81) and (82), and are derived from the analytical solution of a plane wave travelling in free space (see section 3.1.): -

$$E_y\big|_{m,p,q}^{n=0} = E_0\cos\left(\frac{2\pi}{\lambda}|\underline{r}|\right), \quad \mathbf{(81)}$$
$$H_x\big|_{m,p,q}^{n=\frac{1}{2}} = -\frac{E_0}{\nu}\cos\left(\frac{2\pi}{\lambda}|\underline{r}| + \frac{c\Delta t}{2}\right), \quad \mathbf{(82)}$$

where $|\underline{r}| = \left((m\Delta x)^2 + (p\Delta y)^2 + (q\Delta z)^2\right)^{1/2}$. **(83)**

As the FDTD is a leapfrog approach, consideration must be given to the initial conditions to represent this process, in this case we require the initial incident wave to represent the analytical plane wave solution for the electric field at time n=0, and the magnetic field at time n=1/2. Here, the magnetic field is negative so that the correct Poynting vector is obtained such that the initial wave propagates from the outside of the Yee grid towards the object.

When expressions (75), (81) and (82) are combined, the initial electric and magnetic fields are specified by: -

[14]. This is known as up chirping (decreasing λ with time) and down chirping (increasing λ with time). A schematic of these processes is shown in Figure 10: -

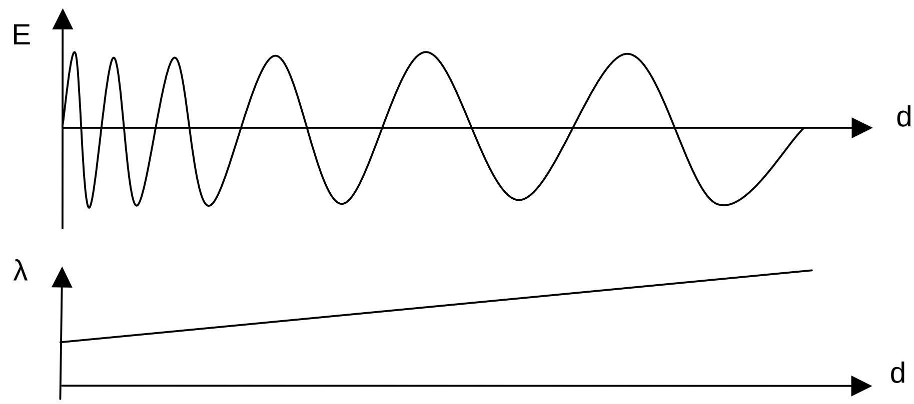

Figure 10: Schematic of a down chirp radio wave

Given that the wavelength of the radio wave through the pulse can be expressed as: -

$$\lambda(d) = \lambda_0 + \lambda' d \text{ ,} \qquad \textbf{(90)}$$

where: -

$\lambda(d) =$ Wavelength at distance d along pulse,
$\lambda_0 =$ Wavelength at front of pulse (d=0),
$\lambda' =$ Rate of change of wavelength with distance (positive or negative).

We can therefore modify equation (84) to include a chirp: -

$$E_x\Big|_{\underline{r}}^{n=} = E \quad (\underline{r}) \quad (\underline{r})(\qquad + \qquad \varphi) \qquad \frac{\pi d(\underline{r})}{\lambda \ + \lambda' d(r)}$$

4.6. Truncation Error

Truncation error is the error introduced into the numerical solution caused by the approximation of using the scheme (in this case the FDTD method) instead of the analytical formula. In this case the truncation error, $\tau^{n}_{m,p,q}$, is expressed mathematically by: -

$$(\quad) = \frac{\partial \quad |_{,\,,}}{\partial} - \frac{\partial \quad |_{,\,,}}{\partial} + \frac{\partial \quad |_{,\,,}}{\partial}$$

$$\left(\quad |_{,\,,} \right) = \frac{|^{1}_{,\,,} - \quad |_{,\,,}}{\Delta} -$$

$$\frac{|^{\frac{1}{2}}_{,\,,\,\frac{1}{2}} - \quad |^{+\frac{1}{2}}_{,\,,\,-\frac{1}{2}}}{\Delta} + \frac{|^{+\frac{1}{2}}_{,\,+\frac{1}{2},} - \quad |^{+\frac{1}{2}}_{,\,-\frac{1}{2},}}{\Delta}$$

$$_{,\,,} \equiv (\quad) - \left(\quad |_{,\,,} \right)$$

$$_{,\,,} = (\quad) - 0_{+}$$

4.7. Stability

The stability condition of the FDTD is given by the Courant condition, which determines the maximum time step to be used given a known grid spacing [1]: -

$$\Delta t \leq c^{-1} \left(\frac{1}{\Delta x^2} + \frac{1}{\Delta y^2} + \frac{1}{\Delta z^2} \right)^{-\frac{1}{2}}. \qquad \textbf{(101)}$$

In the subsequent analysis, we use the expression below for the time step: -

$$\Delta t = 0.9 c^{-1} \left(\frac{1}{\Delta x^2} + \frac{1}{\Delta y^2} + \frac{1}{\Delta z^2} \right)^{-\frac{1}{2}}, \qquad \textbf{(102)}$$

and as we will be using the same grid spacing in each axis ($\Delta x = \Delta y = \Delta z$), this reduces down to: -

$$\Delta t = 0.9 c^{-1} \frac{\Delta y}{\sqrt{3}}, \qquad \textbf{(103)}$$

where we have chosen to define the three grid spacings in terms of the grid spacing along the y-axis.

4.8. Choice of Grid Spacing

5. Plasma Theory

The term plasma refers to a gas which has been excited by some method such that there is a dissociation of electrons from atoms and/or molecules such that charged (positive and negative) and neutral ions exist. The distinguishing feature between plasma and an ordinary ionised

$$F = m\frac{\partial^2 x}{\partial t^2} = Ax\,, \quad \textbf{(105)}$$

where A incorporates the electric permittivity of the region between the electric charges involved. Clearly this equation is that of an oscillatory system, and as such a parameter known as the plasma frequency, ω_f, is introduced to describe this motion. When considering the formation and motion of plasma, it is often considered that the positive/neutral ions within the plasma are stationary, and the electrons are the only particles which exhibit the oscillatory behaviour as described by (105). This is a good approximation as the mass of the electron is 1/1836 that of a hydrogen atom (the lightest constituent of the Earth's atmospheric gases), so that the electrons oscillate rapidly with respect to the other constituents of the plasma.

Plasma is characterised by its Total Electron Content (TEC), which describes the number of free electrons within a given volume, and the collision frequency between ions. The TEC can be used to estimate plasma frequency, using the expression [2]: -

$$\omega_f = \sqrt{\frac{e^2 N_e}{m_e \varepsilon_0}}\,, \quad \textbf{(106)}$$

where ω_f has the units of radians per second, N_e is TEC, m_e is the mass of an electron, e and ε_0 are fundamental constants (electron charge and permittivity of free space respectively).

To determine the effect of an electromagnetic wave incident on a plasma, we must quantify the plasma using the complex permittivity [3], ε_c

where $i = \sqrt{-1}$.

The real part of the complex permittivity, ε'($\underline{r}$), gives the effect of the plasma on the polarisation of the propagating electromagnetic wave, i.e. it gives the relative permittivity of the medium, ε_r. The imaginary part, ε''($\underline{r}$), describes how the amplitude of an incident electromagnetic wave varies as it propagates through the medium, and is related to the conductivity, σ, by: -

$$\varepsilon''(\underline{r}) = \frac{\sigma(\underline{r})}{\omega}, \tag{108}$$

where ω is the frequency of the wave incident on the plasma, expressed in

$$\max(\varepsilon_r) = \varepsilon' \approx 1 - {\frac{10^5}{10^8}}^{2}$$

$$\therefore \max(\varepsilon_r) \approx 0.999999$$

$$\min(\varepsilon_r) = \varepsilon' \approx 1 - {\frac{10^7}{10^8}}^{2}$$

$$\therefore \min(\varepsilon_r) \approx 0.99$$

and as discussed above only the real part of the complex permittivity is considered.

5.2. Group and Phase Velocity in Plasma

A characteristic, and somewhat surprisi

not subject to any external magnetic fields, the dispersion relation for the wave is given by [2]: -

$$\omega^2 = \omega_f^2 + c^2 k^2 \text{.} \tag{113}$$

This equation says that for an electromagnetic wave of a known frequency, ω, incident on plasma, the wave number, k, will reduce as the plasma frequency, ω_f, increases. Ultimately, as the plasma frequency increases and surpasses the frequency of the incident wave, the plasma no longer allows the wave to propagate (k becomes 0 at $\omega_f = \omega$, then imaginary as ω_f increases further). Therefore plasma whose plasma frequency is greater than that of the incident wave appears opaque to the incident wave.

In section 7 we shall examine the variation of the wavelength of a radar pulse in plasma, so for ease of use we rearrange (113) to give the wavelength, λ_p, in the plasma in terms of the plasma frequency: -

$$\lambda_p = \frac{2\pi c}{\left(\omega^2 - \omega_f^2\right)^{1/2}} \text{.} \tag{114}$$

6. Numerical Results from Time Harmonic Problem

6.1. Plane Wave in Free Space

Firstly, we examine the case of an electromagnetic wave propagating through free space and analyse the numerical solution for the evolution of our radar pulse within the computational grid, with the permittivity being equal to ε_0 ($\varepsilon_r = 1$) everywhere in the domain. We examine this case as the analytical solution is known for the whole domain; explicitly that the amplitude, wavelength and spatial extent of the wave will remain constant as it propagates forward.

We take the grid spacing $\Delta x = \Delta y = \Delta z = 0.2$ m, the wavelength $\lambda = 3$ m (100MHz) along with a pulse width, P_w, of 10 m and pulse length, P, of 6 m. Examining the amplitude of the numerical solution for the electric field as time progresses: -

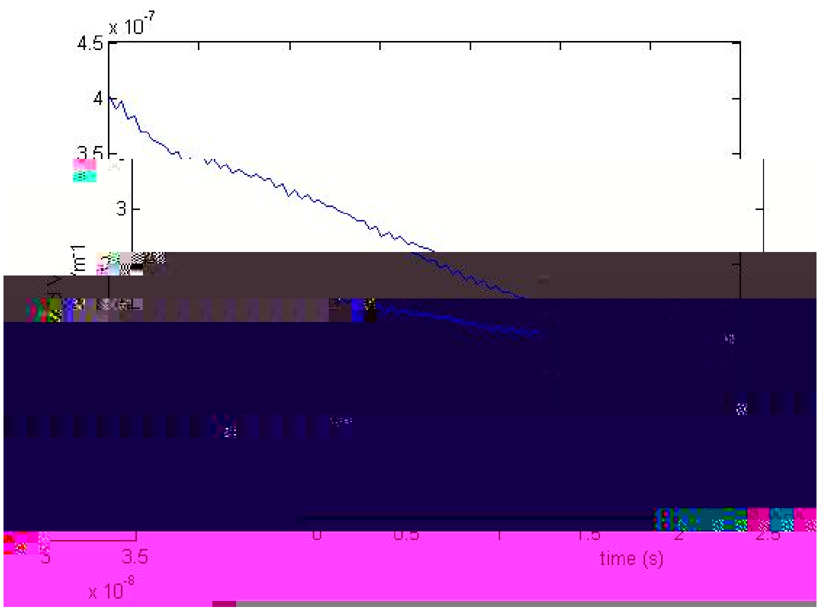

Figure 13: Amplitude of numerical approximation of the electric field of a wave in free space as time progresses

The numerical amplitude reduces with time, and has a rate of change of the order -6.23×10^{-5} $Vm^{-1}ps^{-1}$. This would imply that the initial wave would tend to zero amplitude after 64 ns, i.e. after approximately 190 time steps. Increasing the pulse width of the initial radar pulse region to 15 m: -

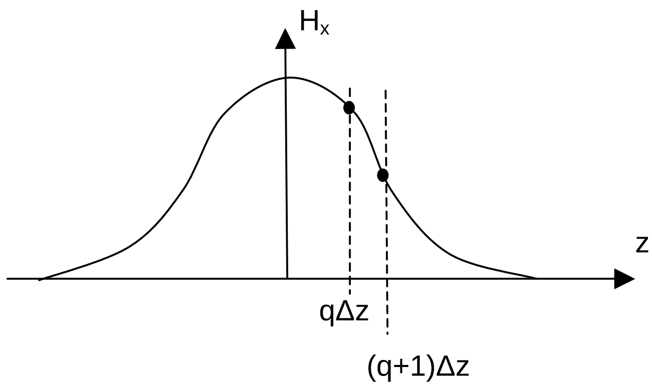

Figure 15: Gaussian distribution schematic

In effect this causes the wave to travel not only in the intended direction (in this case perpendicular to the z-direction) but also to disperse in both the positive and negative z directions as time progresses.

6.2. Plane Wave Incident on a Dielectric Medium

The second case considered is when a radar pulse described by a plane wave is incident on an 'infinite' (extending throughout the whole computational domain in the x-z plane) dielectric medium, described by a constant electric permittivity ε_r. We consider ε_r to take a value of 2, which by using the Snell's laws and Fresnel equations ((28) to (31)) allows a comparison between the analytic to numerical results. The reflected wave when the incident wave is normal to the plane ($\varsigma_i = \varsigma_t = 0$) will have peak amplitude: -

$$| \quad |$$

$$. \qquad \textbf{(117)}$$

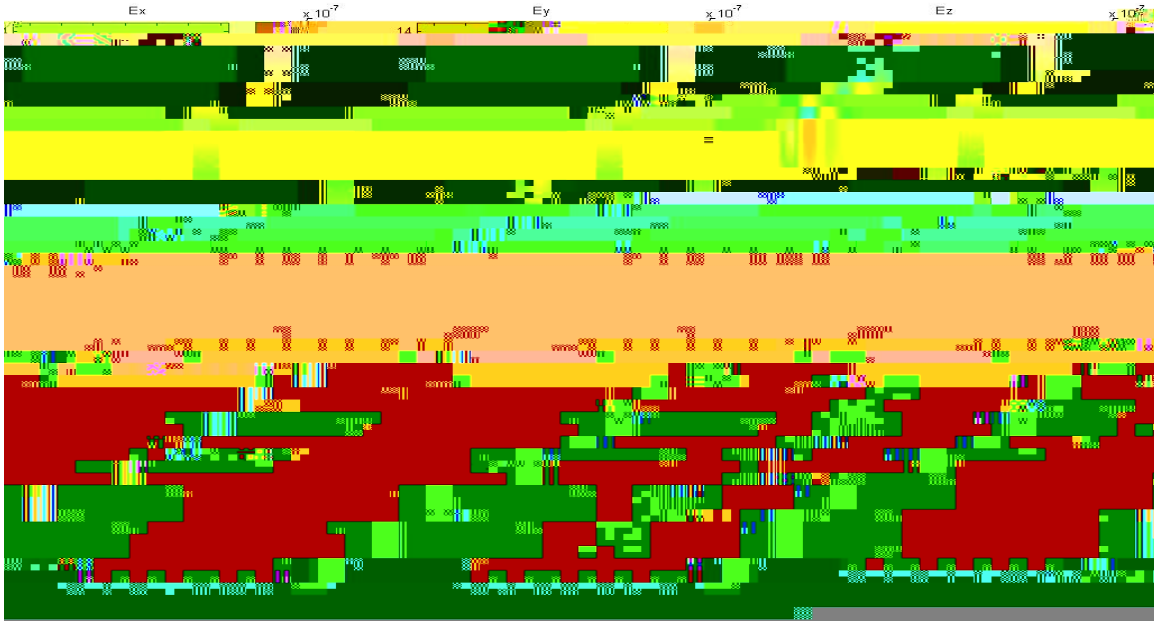

Ex
x 10^-7
Ey
x 10^-7
Ez
x 10^-7

From the figure it can be seen that although there is some agreement between the shape of the electric field for the numerical and analytic solutions, it appears that there has been some reduction in the wavelength and amplitude of the reflected wave. The change in wavelength that has occurred in the numerical solution was assessed to be λ=2.8m (c.f. 3.0 m wavelength incident), this is shown in Figure 19: -

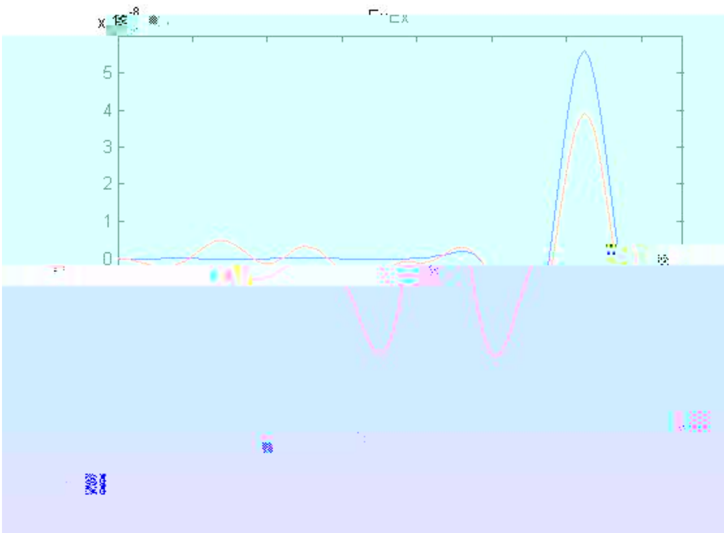

Figure 19: Analytical solution (blue) with λ = 2.8m compared to numerical solution (red) of reflected electric field normally incident on a dielectric (ε_r =2) material.

From this we conclude that the wavelength of the reflected wave off a dielectric is not modelled correctly in the numerical solution. This may be due to the use of the Gaussian function to truncate the radar pulse and is discussed further in 6.3.

The absolute error between the numerical and analytic solution is quantified in Figure 20: -

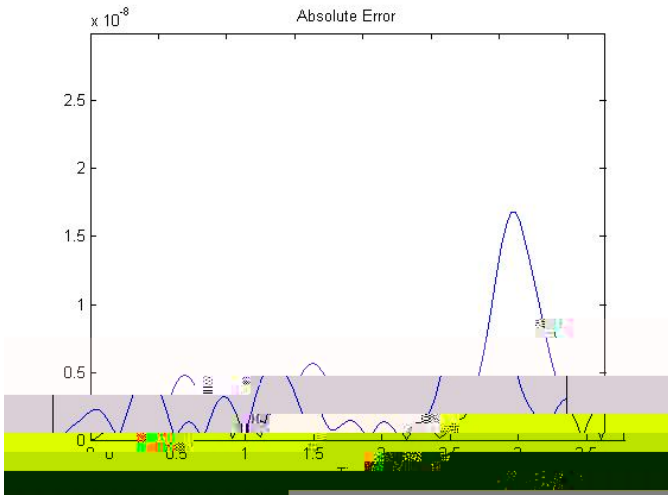

Figure 20: Modulus of absolute error between analytic and numerical solution of reflected electric field

Therefore from this analysis the absolute error of the peak of the wave from the analytical solution is 1.68 $x10^{-8}$ Vm^{-1}, which equates to approximately 30% of the peak amplitude. Additionally the wavelengt

Again it is seen that the wavelength and amplitude of the wave is different for the analytic and numerical solution. The amplitude of the wave in the numerical solution is 44 % below that of the analytical solution. Performing a Fourier Transform (FFT) on the data, we can extract the frequencies that comprise the wave solutions: -

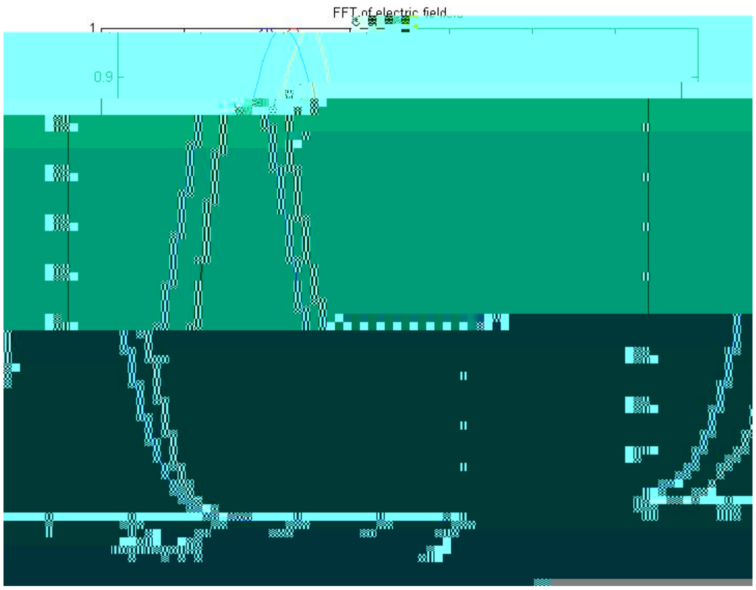

Figure 22: FFT of electric field numerical solution (red) against analytic solution (blue)

From Figure 22 we can see that the numerical solution has higher frequencies within the solution than the analytic solution predicts, with a peak at ~ 116 MHz (0.41 m reduction in wavelength) compared to the input frequency of 100 MHz. To examine this further we halve the grid spacing, Δy, to 0.1 m.

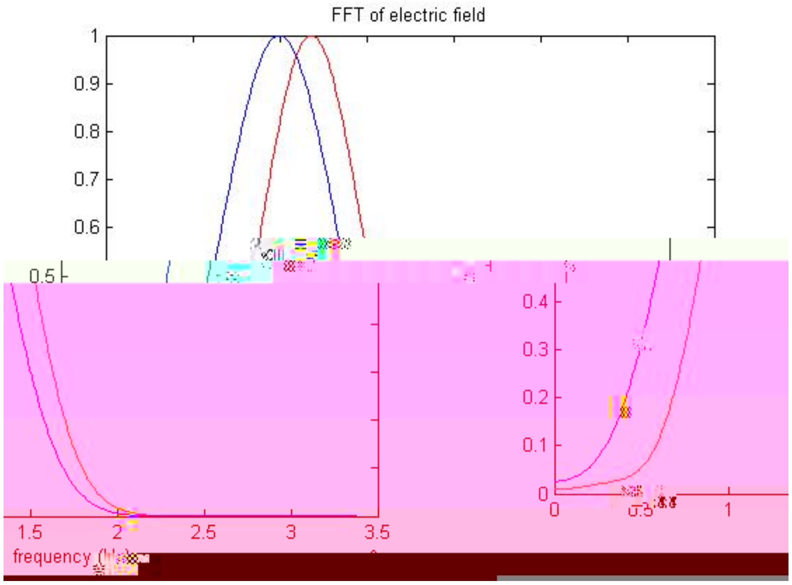

Figure 23: FFT of electric field numerical solution (red) against analytic solution (blue)

In this case there is a peak at the 118 MHz frequency, which equates to a reduction in wavelength of 0.45 m. Therefore reducing the grid spacing has not reduced the error in wavelength of the reflected wave, and therefore may suggest that some aspects of the numerical modelling appear not to be affected by the grid spacing.

7. Numerical Results from non-Time Harmonic Problem

The problem considered in this section is that of the radar signature of an object surrounded by plasma when interrogated by non-time harmonic electromagnetic waves. In particular this will examine the use of a chirped radar pulse to extract information regarding the plasma and object arrangement.

The use of chirp techniques by radar is an attempt to extract additional Doppler information from an observed target [14], and to reduce the vulnerability of the radar to jamming techniques such as chaff. The general arrangement to be considered is shown in Figure 24: -

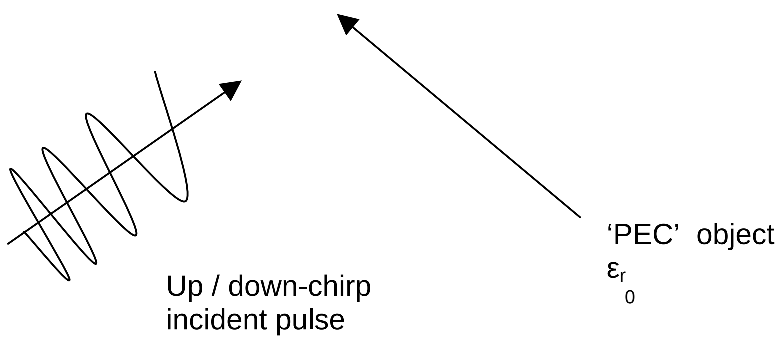

7.1 Incident Wave Representation

The radio wave will have the form of a radar pulse (as described in section 4.4. and utilised in section 6) which is Gaussian shaped both along and perpendicular to the Poynting vector of the electromagnetic fields in the pulse. For the purposes of this section, the wave is now taken to be non-time harmonic with an up-chirp (frequency increases linearly with time within the pulse see section 4.5.). The number of grid points used within the computational grid will be investigated and the effect on the solution (compared to expected behaviour) analysed. Initially a 150 MHz wave with an up-chirp of 250 MHz through the pulse length is considered.

7.2. Grid Spacing Variation

When performing numerical modelling of a sine wave, it is recommended in various texts, such as [1], that as an engineering standard, a minimum of 10 sampling points are required along a single wavelength in order to obtain a 'good' approximation. Using our condition (104) for minimum grid spacing for a dielectric material of relative permittivity ε_r, for the up-chirp wave that gives the recommended resolution of the wave at the 400 MHz ($\lambda = 0.75$ m) upper frequency limit the required grid spacing is: -

$$\{ \quad \sqrt{\ } \quad (\_)$$

To examine the effect of varying the sample rate of the wave on the error within the numerical solution, we examine the variation in wavelength of the transmitted pulse within the plasma. From the theory of electromagnetic waves propagating through a plasma (see section 5.) the wavelength of the wave will vary (specifically elongate), as it enters the plasma region. We will examine how the wavelengths predicted from the numerical solution compare to the wavelengths predicted from the theory for an up-chirped radar pulse. A schematic of the chirped incident wave is shown in Figure 25: -

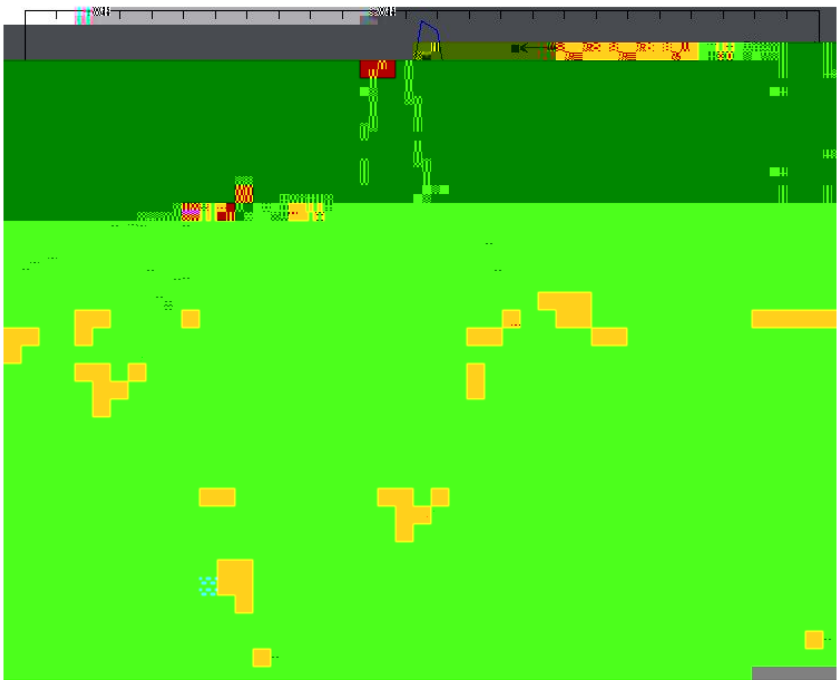

Figure 25: Schematic of the up-chirped incident wave

Examination of the incident wave shows that the points A, B ,C and D are at 1.5 m, 3.55 m, 4.65 m and 5.6 m respectively. The pulse width is kept constant at 14.6 m, and the pulse length is 6.0 m. The time step, Δt, is constant in section of analysis, at 144.44 picoseconds (1.4444×10^{-10} s)

For this analysis, we will assume that the real part of the complex permittivity is constant in the plasma, taking the value 0.25. We also assume the plasma is cold (the imaginary part of the complex permittivity is zero). As the relative permittivity is constant, we make the assumption that the plasma frequency will vary as the radar pulse passes into the plasma region. Therefore we determine the plasma frequency using: -

$$\varepsilon_r = 1 - \frac{\omega_f^2}{\omega^2}$$
$$\Rightarrow \omega_f = \omega\sqrt{1-\varepsilon_r} \quad . \qquad \textbf{(119)}$$

Additionally, an expression for the wavelength of the transmitted wave (λ_f) can be produced based on the wavelength of the incident wave (λ) and relative permittivity:

$$\lambda_f = \frac{2\pi c}{\sqrt{\omega^2 - \omega_f^2}}$$
$$\therefore \lambda_f = \frac{2\pi c}{\sqrt{1-\varepsilon_r}\,\omega}$$
$$\therefore \lambda_f = \frac{\lambda}{\sqrt{1-\varepsilon_r}} \quad . \qquad \textbf{(120)}$$

Given our choice of relative permittivity, in this case $(1-\varepsilon_r)^{½}$ equals 0.5, the wavelength of the wave in the plasma is twice that in free space (the incident wavelength), i.e. $\lambda_f = 2\lambda$. Table 1 details the four points of the incident wave to be considered for the numerical analysis: -

	Point A	Point B	Point C	Point D
Distance along pulse, d (m)	1.5	3.55	4.65	5.6
Wavelength, λ (m)	2.04	1.56	1.08	0.84
Frequency, f (MHz)	147.06	192.31	277.78	357.14
Plasma frequency, f_f (MHz)	127.36	166.55	240.56	309.29
Wavelength in plasma, λ_p (m)	4.08	3.12	2.16	1.68

Table 1: Details of up-chirped pulse incident on cold plasma plane

per iteration. The numerical solution is examined to determine the wavelength of the pulse at points A, B, C and D, and these are compared to those wavelengths predicted from theory. Table 2 shows the results of this analysis: -

Number of sample points at λ_p = 1.5 m	Grid spacing $\Delta x=\Delta y=\Delta z$ (m)	Wavelength from numerical solution at Point A	Wavelength from numerical solution at Point B	Wavelength from numerical solution at Point C	Wavelength from numerical solution at Point D
10	0.15000	4.20	3.20	2.50	2.00
9	0.16667	4.25	3.33	2.50	2.00
8	0.18750	4.31	3.38	2.53	2.06
7	0.21429	4.18	3.43	2.68	2.25
6	0.25000	4.50	3.50	2.75	2.25
5	0.30000	4.50	3.60	3.00	2.40
4	0.37500	4.50	3.94	3.38	3.00
3	0.50000	5.00	4.25	3.50	3.50

Table 2: Recorded wavelengths of numerical solution of wave travelling in plasma

These results are plotted in Figure 26: -

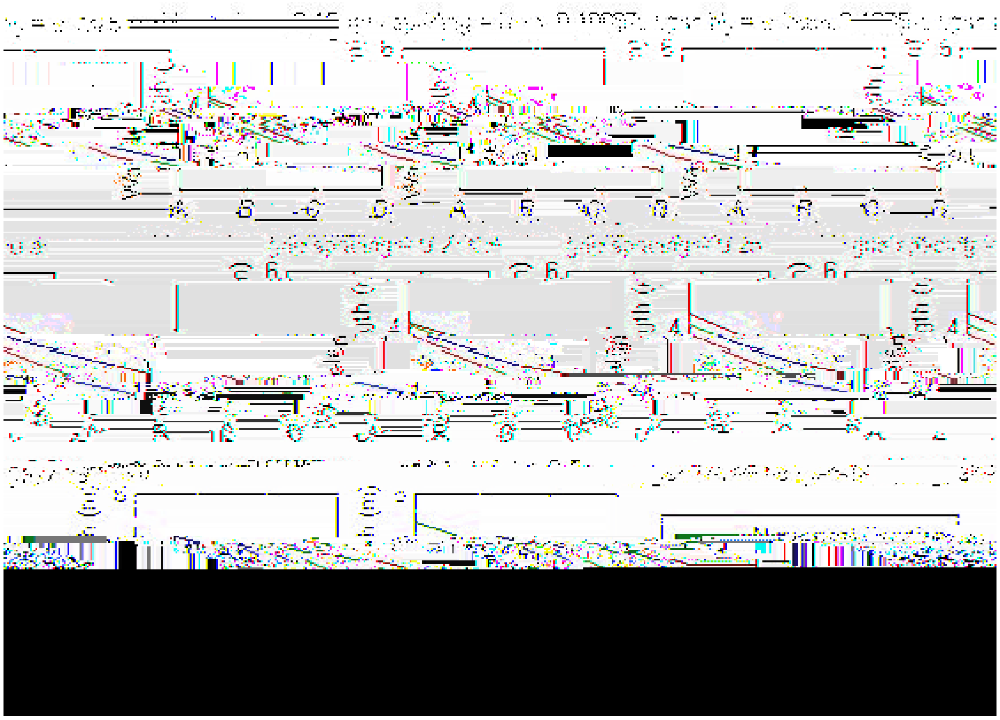

Figure 26: Comparison of wavelengths of chirped pulse extracted from numerical solution to analytical values

These results show a consistent variation of the wavelength in the chirp derived from the numerical solution to the theory at point D (i.e. the high frequency, low wavelength end of the chirp). The slope of the chirp predicted by the numerical solution is consistent with the theory for grid spacing 0.15 to 0.3 m, and it can be seen that when the grid spacing equals 0.375 m, the chirp begins to lose its shape (the gradient of the wavelength varies from the incident wave).

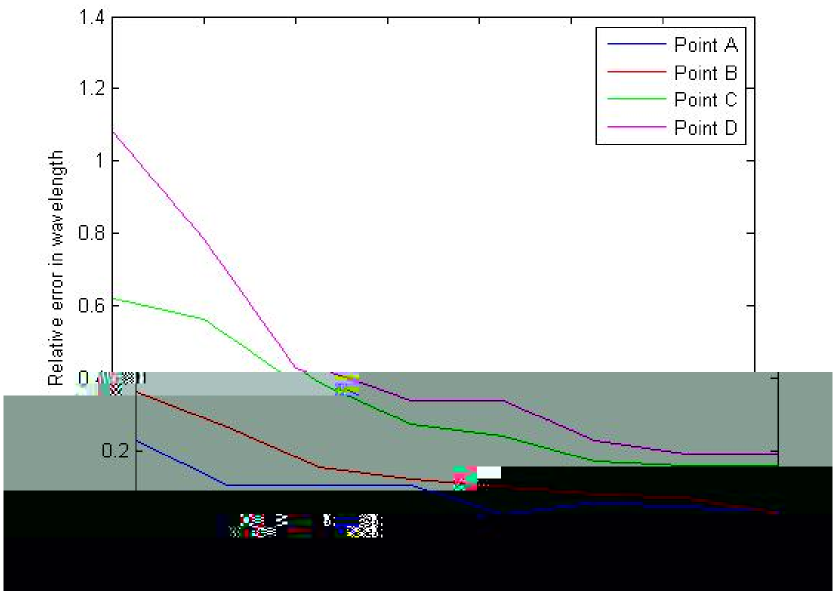

Figure 27: Relative error in wavelength of transmitted wave as grid spacing (and therefore incident wave sampling rate) is varied.

Figure 27 shows that the error in wavelength from the numerical solution increases as the number of points sampling the wave is reduced. Of particular interest is the fact that these four lines are not parallel, that is the error in the chirped wave for the low wavelengths increases as the number of sampling points decreases. This would suggest that there may be some effect by reducing the sampling rate of the wave on the overall error of the solution. However, this must be investigated further as this initial approach involved decreasing the grid eaere may ex.0003 Tc 0.0016 Tw -5.065 0 9(the nps tsj-0)T.A, thtrunc/BBox of thehat.0025 Tw -17

7.3. Variation of Chirp in Incident Wave

We now consider an incident wave on a plane of plasma (with fixed electric permittivity of 0.25) with a significant amount of chirp to see the error in the

Peak Number	Wavelength (m)	Distance (m), t=2.0216x10^{-8} s	Distance (m), t=2.3104x10^{-8} s	Phase Velocity (multiples of c)	Error in phase velocity (multiples of c)
1	0.6389	10.575	12.3	1.9910	-0.0090
2	0.687	9.925	11.65	1.9910	-0.0090
3	0.7909	9.175	10.9	1.9910	-0.0090
4	0.8449	8.4	10.15	2.0199	0.0199
5	0.9469	7.5	9.275	2.0487	0.0487
6	1.044	6.55	8.275	1.9910	-0.0090
7	1.18	5.475	7.2	1.9910	-0.0090
8	1.319	4.3	6.075	2.0487	0.0487
9	1.505	3.025	4.775	2.0199	0.0199
10	1.741	1.6	3.4	2.0776	0.0776

Table 3: Examination of phase velocities recorded from numerical solution of the electromagnetic wave in the plasma

The phase velocities recorded from the numerical solution have a mean of 2.0170c, with a standard deviation 0.0318c. The phase velocities for the low wavelengths tend to be lower than predicted, and for the higher wavelengths are greater than predicted. Figure 29 summarizes these findings in terms of the sampling rate of the incident wave and t

There appears to be some increase in error of phase velocity as the number of sampling points of the incident wave increases to 11.6 points per wavelength. The numerical solution for the other points is within 2.5% of the actual phase velocity predicted by theory; this is discussed further in 7.4.

The wavelengths within the chirped pulse were extracted by examining the difference in distance along the y-axis of adjacent peaks in the numerical solution, as shown in Figure 30: -

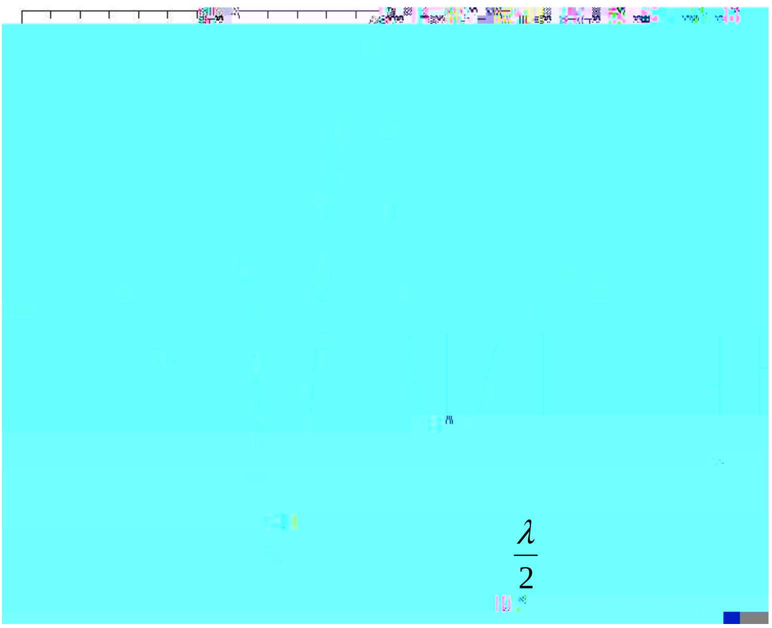

Figure 30: Schematic of wavelength measurement

A comparison of the wavelengths of the analytic solution to the numerical solution is shown in Figure 31: -

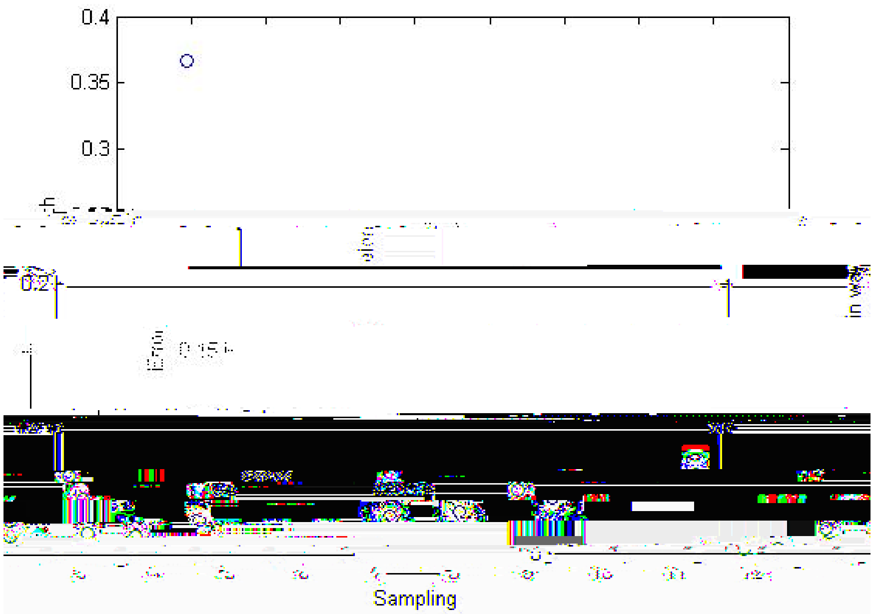

Figure 31: Relative error in wavelength (in meters) against sampling rate of incident wave (points per wavelength)

From Figure 31 it can be seen that for the chirped wave regions sampled at greater than 4 points per wavelength, the wavelength from the numerical solution is within 5 % of that predicted analytically. Below this sampling rate, the numerical solution shows significant deviation from theory reporting a wavelength with a relative error of 37%. In general there is also an increase in relative error T(hereaeretwog ps

7.4. Conclusions

From the analysis in this section, it is concluded that the use of a Yee grid and finite radar pulse has utility in accurately modelling the behaviour of chirped electromagnetic waves in plasma. The minimum number of sampling points required to use this approach is assessed to be 4 points per wavelength at the high frequency end of the chirp. Numerical results in this region for the wavelength and phase velocity of the wave propagating in the plasma are within 5 % and 4 % of the analytical solution respectively. No examination of the group velocity has been made in this analysis, and is left as an area for future research.

8. Summary

The research within this report has shown that the FDTD has the utility to model the propagation of electromagnetic waves in various media. When modelling finite radar pulses rather than infinite, time-harmonic incident fields, careful consideration must be given to the shape and composition of the numerical grid and initial conditions, in particular to reduce the dispersion of the pulse perpendicular to the direction of motion. In this report a Gaussian function has been utilised to set up a continuous, and differentially continuous, incident pulse; which may be up or down chirped.

Numerical results for a time harmonic wave propagating in free space show a reduction in the peak amplitude of the electric field of up to 0.5% per time step, although this rate is reduced by 35% when the pulse width was doubled.

Analysis of the numerical solutions from the examples considered has shown the method used in this report can predict electric field peak amplitudes (as predicted by Snell's law/Fresnel equations) of a reflected wave off a dielectric surface to within approximately 60% percent. This accuracy is dependent on the angle of incident on the wave, grid spacing chosen and dimensions of the pulse as defined in the examples in section 6. Due to the size of this error, this method is not recommended for use in determining RCS values of dielectrics, due to the requirement to accurately determine reflected electric field amplitudes. Additionally a systematic error in the wavelength of the radio wave reflected off a dielectric was observed, which may be due to the use of a Gaussian function along the length of the pulse, though further research is required to confirm this.

An investigation into the required resolution of the modelled chirped radar pulse (incident on a plasma) to produce numerical results which are consistent with electromagnetic theory has shown that a sampling rate of four points per wavelength appears to be sufficient to ensure the phase information and phase velocity of the transmitted pulse is recoverable from the numerical solution. From the results there appears to be some increase in error of the plasma wavelength as the number of sampling points increases. It is postulated that this is due either to the use of a Gaussian function in the pulse or due to an error induced in the methodology of measuring the wavelength in the solution.

The use of a Gaussian function to truncate an infinite sine wave so that a finite radar pulse in space can be represented numerically appears to be problematic. The analysis in this report has shown that the numerical solution for a finite pulse propagating in a dielectric/plasma exhibits dispersion as the computation progresses forward in time. Dispersion of the electric field is observed tangentially to the direction of propagation of the wave.

Future work in this area would be to investigate different finite difference formulations of Maxwell’s equations, and assess their capability to model non-

9. References

1. The Finite Difference Time Domain Method for Electromagnetics, K. S. Kunz and R. J. Luebbers,1993.
2. Introduction to Plasma Physics, F. F. Chen, 1974.
3. Basic Electromagnetism, E. R. Dobbs, 1993.
4. Radar Cross Section handbook, Volume 2, Ruck et al, 1970.
5. Introduction to Radar Systems, Third Edition, M. I. Skolnik, 2001.
6. Relative Accuracy of Several Finite-Difference Time-Domain Methods in Two and Three Dimensions. K. L. Shalager et al, IEEE, Vol. 41, No. 12 (1993) pg 1732 – 1737.
7. A New Finite-Difference Time-Domain Algorithm for the Accurate Modelling of Wide-Band Electromagnetic Phenomena, S. R. Omick, S. P. Castillo, IEEE, Vol. 35, No. 2 (1993) pg 215 – 222.
8. Numerical research on the RCS of plasma, Z. Yu et al, IEEE, (2003) pg 428 – 432.
9. Three-Dimensional Computation of Reduction in Radar Cross Section Using Plasma Shielding, B. Chaudhury, S. Chaturvedi, IEEE, Vol. 33, No. 6, (2005), pg 2027 – 2034.
10. The Calculation of Back-Scattering Radar cross Section of Plasma Spheres, Y. Gao et al., 25th International Conference on Infrared and Millimeter Waves, 2000, pg 415 – 416.
11. Absorbing Boundary Conditions for the Finite-Difference Approximation of the Time-Domain for Electromagnetic-Field Equations, G. Mur, IEEE, Vol. EMC-23, No. 4, (1981), pg 377 – 382.
12. Ionospheric Radio, K. Davies, 1990.
13. Numerical Solution of Initial Value Problems involving Maxwell's Equation in Isotropic Media, K. S. Yee, IEEE, Vol. 14, (1966), pg 302.
14. Modern Radar Systems, H. Meikle, 2001.

Appendix A: Vector identities

Lemma 1

$$\nabla \cdot \nabla \times \underline{A} = 0$$

Proof

$$\nabla \times \underline{A} = \begin{vmatrix} \underline{i} & \underline{j} & \underline{k} \\ \frac{\partial}{\partial x} & \frac{\partial}{\partial y} & \frac{\partial}{\partial z} \\ A_x & A_y & A_z \end{vmatrix} =$$

$$\underline{i}\left(\frac{\partial A_z}{\partial y} - \frac{\partial A_y}{\partial z}\right) + \underline{j}\left(\frac{\partial A_x}{\partial z} - \frac{\partial A_z}{\partial x}\right) + \underline{k}\left(\frac{\partial A_y}{\partial x} - \frac{\partial A_x}{\partial y}\right) = \underline{B} \quad ,$$

$$\_ \quad \frac{}{} \quad \frac{}{} \quad \frac{}{}$$

$$\_ \quad \frac{}{} \quad \frac{A}{y} \quad \frac{A}{z} \qquad \frac{}{y} \quad \frac{A}{z} \quad \frac{A}{x} \qquad \frac{}{z} \quad \frac{A}{x} \quad \frac{A}{y}$$

$$\frac{A}{x \ y} \quad \frac{A}{x \ z} \quad \frac{A}{y \ z} \quad \frac{A}{y \ x} \quad \frac{A}{z \ x} \quad \frac{A}{z \ y}$$

Lemma 2

$$\nabla \times (\nabla \times \underline{A}) = -\nabla^2 \underline{A} + \nabla(\nabla \cdot \underline{A})$$